Using the de Rham sequence for accelerating mixed finite element computations

Jeferson Wilian Dossa Fernandes[1], Sonia Maria Gomes[2], Philippe Remy Bernard Devloo[3]

[1]*Centro de Estudos de Petróleo (CEPETRO)-Universidade Estadual de Campinas*
Rua Cora Coralina, 350, Campinas-SP, Brazil
jwdf@unicamp.br
[2]*IMECC-Universidade Estadual de Campinas*
Campinas-SP, Brazil
soniag@ime.unicamp.br
[3]*FEC - Universidade Estadual de Campinas*
R. Josiah Willard Gibbs, 85, 13083-839, Campinas-SP, Brazil
phil@fec.unicamp.br

Abstract. Mixed finite element computations arise in the simulation of multiple physical phenomena. Due to its characteristics, such as the strong coupling between the approximated variables, the solution of such class of problems may suffer from numerical instabilities as well as a computational cost. The de Rham diagram is a standard tool to provide approximation spaces for the solution of mixed problems as it relates H^1-conforming spaces with $H(curl)$ and $H(div)$-conforming elements in a simple way by means of differential operators. This work presents an alternative for accelerating the computation of mixed problems by exploring the de Rham sequence to derive divergence-free functions in a robust fashion. The formulation is numerically verified for the 2D case by means of benchmark cases to confirm the theoretical regards.

Keywords: Mixed formulation, Divergence-free functions, de Rham sequence.

1 Introduction

Several problems in engineering, when treated by finite element approximations, may result in mixed problems. In geomechanics, specifically, one may cite groundwater flow [1, 2] soil-structure interaction [3], reservoir simulations [4], among others. In the literature, this class of formulations is named as "mixed" because more than one field is approximated and usually one of them plays the role of Lagrange multipliers [5] and the approximation of such class of problems may be performed by many different approaches.

In this work, we propose a strategy to explore the properties from the de Rham sequence in order to accelerate the computation of mixed finite element problems. The de Rham sequence is given by

$$\mathbb{R} \longrightarrow H^1(\Omega) \overset{grad}{\longrightarrow} H(curl,\Omega) \overset{curl}{\longrightarrow} H(div,\Omega) \overset{div}{\longrightarrow} L^2(\Omega) \longrightarrow \{0\}, \tag{1}$$

and relates H^1-conforming elements with $H(curl)$-conforming and $H(div)$-conforming elements via differential operators (see for instance [6]). By the de Rham sequence it is well known that the curl of $H(curl)$ functions maps to the null space of $H(div)$ spaces, meaning that all $\boldsymbol{\psi} \in H(div)$ functions whose $\nabla \cdot \boldsymbol{\psi} = 0$ can be represented by a linear combination of the curl of $H(curl)$ functions. This property can be extended to finite dimensional spaces if those are constructed in a balanced way, as is the case of the basis functions in NeoPZ [7] environment, the computational tool employed in this work.

In this paper, we demonstrate that divergence-free approximations can be obtained by means of H^1-conforming spaces. This class of functions is applied for solving the mixed version of the Laplace's problem. In addition, we perform some numerical experiments to demonstrate that these approximations leads to results identical to the ones obtained by standard $H(div)$ approximations of equivalent polynomial order.

The paper is organized as follows: in section 2 we describe the divergence-free functions in 2D followed by the weak formulation employing this family of functions as well as computational implementation aspects. In section 3 we present preliminary results for the benchmark five-spot problem. Conclusions and perspectives are drawn in section 4.

2 Formulation

2.1 Divergence-free functions in 2D

Firstly, consider the function $\boldsymbol{\phi} = \phi(x,y)\mathbf{e}_z \in H(curl,\Omega)$, where $\mathbf{e}_x, \mathbf{e}_y$ and $\mathbf{e}_z$ are the unit vectors forming the canonical base, $\phi(x,y)$ is an arbitrary scalar function and $\Omega \subset \mathbb{R}^d$ is an open-bounded region with boundary $\partial\Omega = \partial\Omega_D \cup \partial\Omega_N$, with $\partial\Omega_D$ and $\partial\Omega_N$denoting the parts where Dirichlet and Neumann conditions are enforced, respectively. Thus, it follows that $\boldsymbol{\psi}$, the curl of $\boldsymbol{\phi}$, is given by

$$\boldsymbol{\psi} = \nabla\times\boldsymbol{\phi} = \nabla\times(\phi\,\mathbf{e}_z) = \frac{\partial\phi}{\partial y}\mathbf{e}_x - \frac{\partial\phi}{\partial x}\mathbf{e}_y. \tag{2}$$

From the de Rham diagram 1 it follows the property that $\nabla\cdot\boldsymbol{\psi} \equiv 0$. $\boldsymbol{\psi}$-type functions are denoted as divergence-free and thus $\boldsymbol{\psi} \in H(div,\Omega)$.

2.2 Weak form

In this section we apply the divergence-free functions to the mixed approximation of Laplace's equation whose problem reads: find $\boldsymbol{\sigma} \in H(div,\Omega)$ and $p \in L^2(\Omega)$, respectively flux and pressure fields, such that

$$\begin{aligned} K^{-1}\boldsymbol{\sigma} + \nabla p &= 0 \\ \nabla\cdot\boldsymbol{\sigma} &= 0 \end{aligned}, \tag{3}$$

with

$$\begin{aligned} p(s) &= p_D \;\; s \in \partial\Omega_D, \\ \boldsymbol{\sigma}(s)\cdot\mathbf{n} &= \mathbf{g}_N(s) \;\; s \in \partial\Omega_N, \end{aligned} \tag{4}$$

where K^{-1} is the permeability tensor, $\boldsymbol{n}$is the outward unit vector normal to $\partial\Omega$ and $p_D$and $\mathbf{g}_N$are given functions.

Consider the infinite dimension function spaces given by

$$W = \{\boldsymbol{\psi} \in H(div,\Omega); \nabla\cdot\boldsymbol{\psi} = 0\} \tag{5}$$

and

$$Z = \left\{z \in L^2(\Omega)\right\}, \tag{6}$$

and their finite-dimensional version denoted by the superscript h, the characteristic length of a given finite element discretization. Notice that W is the divergence-free subset of $H(div,\Omega)$.

The weak statement of (3)-(4) for the finite dimensional space, obtained by means of Gakerkin's method, reads as follows: find $p^h \in Z^h$ and $\boldsymbol{\sigma}^h \in W^h$, with $\boldsymbol{\sigma}(s)\cdot\mathbf{n} = \mathbf{g}_N(s)$, such that

$$\int_\Omega \boldsymbol{\psi}^h\cdot\left(K^{-1}\boldsymbol{\sigma}^h\right)d\Omega - \int_\Omega \nabla\cdot\boldsymbol{\psi}^h p d\Omega = -\int_{\partial\Omega_D} p_D\left(\boldsymbol{\psi}^h\cdot\mathbf{n}\right)d\partial\Omega_D - \int_{\partial\Omega_N}\boldsymbol{\psi}^h\cdot\mathbf{g}_N\,d\partial\Omega_N \quad \forall\boldsymbol{\psi}^h \in W^h, \tag{7}$$

$$\int_\Omega z^h\nabla\cdot\boldsymbol{\sigma}^h d\Omega = 0 \qquad \forall z^h \in Z^h. \tag{8}$$

From (5), it follows that $\nabla\cdot\boldsymbol{\sigma}^h \equiv 0$ and $\nabla\cdot\boldsymbol{\psi}^h \equiv 0$ and then the weak form can be written as

$$\int_\Omega \boldsymbol{\psi}^h\cdot\left(K^{-1}\boldsymbol{\sigma}^h\right)d\Omega = -\int_{\partial\Omega_D} p_D\left(\boldsymbol{\psi}^h\cdot\mathbf{n}\right)d\partial\Omega_D - \int_{\partial\Omega_N}\boldsymbol{\psi}^h\cdot\mathbf{g}_N\,d\partial\Omega_N. \tag{9}$$

Inserting (2) onto (9) one obtain

$$\int_{\Omega} \boldsymbol{\psi}_i^h \cdot \left(K^{-1}\boldsymbol{\psi}_j^h\right) d\Omega \left\{\bar{\boldsymbol{\sigma}}_j^h\right\} = -\int_{\partial\Omega_D} p_D \left(\boldsymbol{\psi}_j^h \cdot \mathbf{n}\right) d\partial\Omega_D - \int_{\partial\Omega_N} \boldsymbol{\psi}_j^h \cdot \mathbf{g}_N \, d\partial\Omega_N, \tag{10}$$

$$\int_{\Omega} \left\{\frac{\partial\phi_i^h}{\partial y}\mathbf{e}_x - \frac{\partial\phi_i^h}{\partial x}\mathbf{e}_y\right\} \cdot \left(K^{-1}\left\{\frac{\partial\phi_j^h}{\partial y}\mathbf{e}_x - \frac{\partial\phi_j^h}{\partial x}\mathbf{e}_y\right\}\right) d\Omega \left\{\bar{\boldsymbol{\sigma}}_j\right\} = -\int_{\partial\Omega_D} p_D \left(\boldsymbol{\psi}_j^h \cdot \mathbf{n}\right) d\partial\Omega_D - \int_{\partial\Omega_N} \boldsymbol{\psi}_j^h \cdot \mathbf{g}_N \, d\partial\Omega_N, \tag{11}$$

$$\int_{\Omega} \nabla\phi_i^h \left(K^{-1}\nabla\phi_j^h\right) d\Omega \left\{\bar{\boldsymbol{\sigma}}_j\right\} = -\int_{\partial\Omega_D} p_D \left(\boldsymbol{\psi}_j^h \cdot \mathbf{n}\right) d\partial\Omega_D - \int_{\partial\Omega_N} \boldsymbol{\psi}_j^h \cdot \mathbf{g}_N \, d\partial\Omega_N, \tag{12}$$

where i, j are indexes of nodal variables and $\{\bar{\boldsymbol{\sigma}}_j\}$ is the vector of flux nodal values.

As may be noticed, once $\phi \in H^1$ the introduction of divergence-free functions onto the mixed formulation results in a bilinear operator equivalent to the H^1 approximation of the Laplace's equation, with proper boundary conditions.

3 Numerical tests

This section presents two numerical tests with the proposed divergence-free functions. Both cases are simulated with quadrilateral finite elements, polynomial order = 2 (notice that it implies polynomial order 3 for ϕ in Eq. (9)) and are compared to the standard mixed $H(div)$ approach. The results are evaluated by means of the flux L^2 norm given by

$$||\boldsymbol{\sigma} - \boldsymbol{\sigma}_h||_{L^2} = \int_{\Omega_h} (\boldsymbol{\sigma} - \boldsymbol{\sigma}_{DF}) \, d\Omega_h. \tag{13}$$

3.1 Test 1 - Polynomial analytic solution

The problem consists in a square domain $\Omega = [0,0] \times [1,1]$ with analytic solution $p = x^3y - y^3x$ and $\boldsymbol{\sigma} = K\left[\left(y^3 - 3x^2y\right)\mathbf{e}_x + \left(3y^2x - x^3\right)\mathbf{e}_y\right]$. The permeability tensor is taken as the identity matrix and the plots of both fields are presented in Fig. 1.

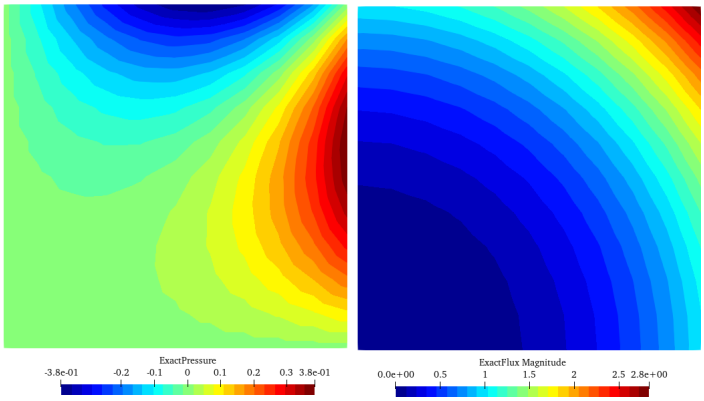

Figure 1. Test 1 - Exact pressure and flux (magnitude) fields.

The numerical tests are carried by taking the exact solution for enforcing Dirichlet and/or Neumann boundary conditions, with a 10x10 structured finite element mesh. The first test consists in simulate the problem with different combinations of boundary conditions, which are presented in Table 1.

As can be noticed, a loss of accuracy can be observed when applying both Dirichlet and Neumann boundary conditions in different portions of the boundary. This problem is related to numerical instabilities when solving the resulting problem with Neumann boundary conditions enforced by means of a penalization technique, which turned the convergence dependent on the penalization parameter.

The use of hybridized formulations [8, 9] in combination with static condensation [10, 11] is a wide known strategy on finite element codes to both reduce the size of the final algebraic system and produce a locally conservative method. Then, to overcome drawback described in the previous paragraph an hybridization technique

Configuration	$\|\|\sigma - \sigma_{DF}\|\|_{L^2}$	$\|\|\sigma - \sigma_{H(div)}\|\|_{L^2}$
All boundaries Dirichlet	2.672612419123790e-05	2.672612419124198e-05
Neumann BC in the upper edge	2.672612419123695e-05	2.672612419124208e-05
Neumann BC in the upper and lower edges	2.808233896848702e-05	2.672612419124665e-05
Neumann BC in the upper lower and left edges	2.672612419124693e-05	2.672612419124956e-05
All boundaries Neumann	2.672612419125250e-05	2.672612419125112e-05

Table 1. Test 1 - Approximation error.

is applied, so the Neumann boundary conditions can also be weakly enforced. The results obtained with the hybridization technique are presented in Table 2, where no instabilities are observed.

Configuration	$\|\|\sigma - \sigma_{DF}\|\|_{L^2}$	$\|\|\sigma - \sigma_{H(div)}\|\|_{L^2}$
All boundaries Dirichlet	2.672612419123790e-05	2.672612419124198e-05
Neumann BC in the upper edge	2.672612419124245e-05	2.672612419124208e-05
Neumann BC in the upper and lower edges	2.672612419124286e-05	2.672612419124665e-05
Neumann BC in the upper lower and left edges	2.672612419124528e-05	2.672612419124956e-05
All boundaries Neumann	2.672612419124323e-05	2.672612419125112e-05

Table 2. Test 1 - Approximation errors with hybridized Neumann boundary conditions.

Test 2 - A benchmark: the five-spot problem

The second numerical test is the well known five-spot benchmark problem. It simulates the flow of a reservoir with equally spaced injection and production wells. The problem has exact solution given by

$$p\left(x,y\right) = \log\left(\sqrt{x^2+y^2}\right) - \log\left(\sqrt{\left(x-d\right)^2+\left(y-d\right)^2}\right) \\ - \log\left(\sqrt{\left(x+d\right)^2+\left(y-d\right)^2}\right) - \log\left(\sqrt{\left(x-d\right)^2+\left(y+d\right)^2}\right) - \log\left(\sqrt{\left(x+d\right)^2+\left(y+d\right)^2}\right),$$

where d is the distance between injection and production wells, which for the adopted domain $\Omega = [0,0] \times [1,1]$ is equal to the unity. To avoid cumbersome expressions, the flux exact solution can be directly by $\boldsymbol{\sigma} = K\nabla p$.

This case is simulated with the finite element mesh illustrated in Fig. 2, with 1140 finite elements. Again, boundary conditions are set from the analytical expressions and the permeability tensor is taken as the identity matrix. Injection and production wells are represented in the spatial discretization by semicircles with radius 0.05 units. Both exact flux and pressure fields are also presented in Fig. 2.

Analogously to the first test, this case was evaluated for different configurations of boundary conditions, initially not hybridized. Results are presented in Table 3.

As can be noticed, the same numerical instabilities are observed in this case, which as presented in Table 4, can be again avoided by using the hybridization technique on the Neumann boundary conditions.

Finally, a last numerical test is to extend the concept of hybridization also to the domain. It means that all finite elements are disconnected and, after the static condensation procedure, the final system of algebraic equations has the size of the introduced Lagrange multipliers (λ^h), responsible for the connection between the elements [9].

Several alternatives can be proposed in this sense. In our tests, 8 scenarios were evaluated (described in Table 5), including standard mixed $H(div)$ and hybridized divergence-free functions. It is worthwhile mention that compatible polynomial order needs to be employed to the Lagrange multiplier field, which corresponds to scenarios 4-6 and 8 (for the boundary conditions only). In scenarios 7 and 8 the domain hybridization is performed with a possibly lower cost alternative (in terms of numerical integration), with constant Lagrange multipliers. The error analysis for all scenarios is presented in Table 6.

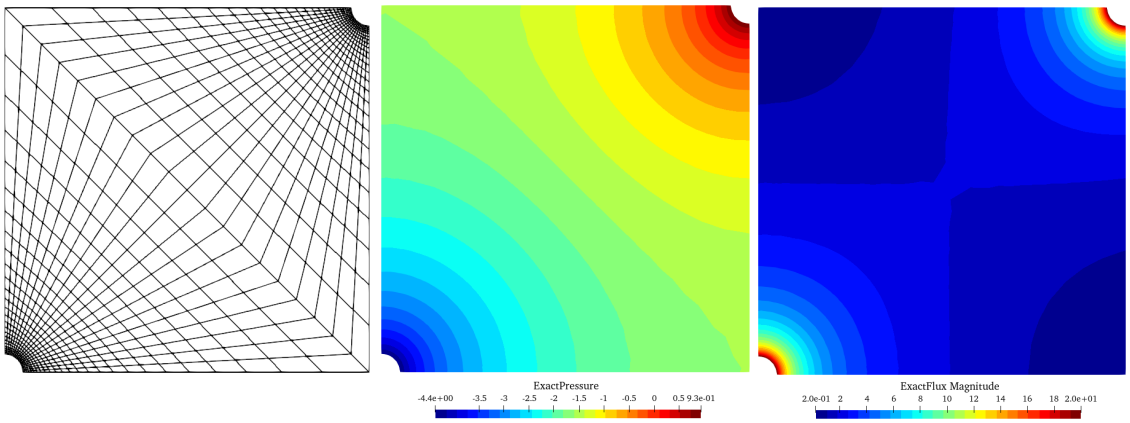

Figure 2. Finite element mesh for the five-spot benchmark

Configuration	$\|\|\sigma - \sigma_{DF}\|\|_{L^2}$	$\|\|\sigma - \sigma_{H(div)}\|\|_{L^2}$
All Dirichlet BC	3.421201755805085e-05	3.49215783010819e-05
1 well Neumann BC	3.421202011271095e-05	3.49179192926942e-05
Both wells Neumann BC	1.696853946870948e-03	3.49142599018502e-05
Both wells +Bottom	4.702552582222026e-04	3.47531302702461e-05
Both wells +Bottom+Top	1.085095943403631e-03	3.45729264067967e-05
Both wells +Bottom+Top+Left	3.421874332893253e-05	3.44082498054288e-05
All boundaries Neumann	3.421874332893253e-05	3.42242710057238e-05

Table 3. Test 2 - Approximation error.

Configuration	$\|\|\sigma - \sigma_{DF}\|\|_{L^2}$	$\|\|\sigma - \sigma_{H(div)}\|\|_{L^2}$
All Dirichlet BC	3.421201755805085e-05	3.49215783010819e-05
1 well Neumann BC	3.421203147649551e-05	3.49179192926942e-05
Both wells Neumann BC	3.421204539481118e-05	3.49142599018502e-05
Both wells +Bottom	3.421340823747712e-05	3.47531302702461e-05
Both wells +Bottom+Top	3.421864568239351e-05	3.45729264067967e-05
Both wells +Bottom+Top+Left	3.421952134609415e-05	3.44082498054288e-05
All boundaries Neumann	3.422427091598586e-05	3.42242710057238e-05

Table 4. Approximation error - Hybridized BC

The last numerical test have shown that divergence-free functions can be explored in a wide range of approaches in order to obtain a lower cost solution for mixed problems with the same accuracy of $H(div)$-conforming spaces, denoted specially by the considerable lower number of degrees of freedom in the arising matrix problem.

4 Conclusions

In this paper we presented a formulation to approximate the solution of the 2D mixed Laplace problem by means of the construction of divergence-free space functions by taking advantage of the de Rham sequence properties. The results obtained in a first step have shown numerical instabilities when the problem to be solved presented boundary conditions of Neumann type enforced by a penalization manner. This issue was overcome by means of the boundary condition hybridization. In this case all results presented the same numerical approximation as standard $H(div)$ function spaces of compatible polynomial order with a lower computational cost. A last

Scenario	Approximation space	Boundary conditions	Hybridization
1	$H(div)$	All Dirichlet	No
2	$H(div)$	All Neumann	No
3	Divergence-Free	All Dirichlet	No
4	Divergence-Free	All Neumann	Boundary conditions
5	Divergence-Free	All Dirichlet	Domain
6	Divergence-Free	All Neumann	Boundary conditions + Domain
7	Divergence-Free	All Dirichlet	Domain (constant λ)
8	Divergence-Free	All Neumann	Boundary conditions + Domain (constant λ)

Table 5. Test 2 - Hybridization scenarios

Scenario	Degrees of freedom	$\|\|\sigma - \sigma_h\|\|_{L^2}$
1	27210	3.49215783010819e-05
2	27210	3.42242710057238e-05
3	5093	3.42120175580508e-05
4	5513	3.42242709159859e-05
5	5790	3.42120175566171e-05
6	6210	3.42242671258764e-05
7	5790	3.42120175581107e-05
8	6210	3.42242711370172e-05

Table 6. Test 2 - Error analysis for the hybridized formulation.

numerical test also presented different usages of divergence-free class of functions. In future work the formulation may be explored for 3D simulations. In addition, preliminary results have shown that the presented approximation have advantageous spectral properties that will be explored as a preconditioner for different numerical applications such as porous media flows.

Acknowledgements. The authors thankfully acknowledge the financial support from Equinor and FAPESP, Brazil - Fundação de Amparo à Pesquisa do Estado de São Paulo, Brazil (grant 2021/02187-7).

Authorship statement. The authors hereby confirm that they are the sole liable persons responsible for the authorship of this work, and that all material that has been herein included as part of the present paper is either the property (and authorship) of the authors, or has the permission of the owners to be included here.

References

[1] L. Traverso, T. Phillips, and Y. Yang. Mixed finite element methods for groundwater flow in heterogeneous aquifers. *Computers & Fluids*, vol. 88, pp. 60–80, 2013.

[2] I. Berre, W. M. Boon, B. Flemisch, A. Fumagalli, D. Gläser, E. Keilegavlen, A. Scotti, I. Stefansson, A. Tatomir, K. Brenner, S. Burbulla, P. Devloo, O. Duran, M. Favino, J. Hennicker, I.-H. Lee, K. Lipnikov, R. Masson, K. Mosthaf, M. G. C. Nestola, C.-F. Ni, K. Nikitin, P. Schädle, D. Svyatskiy, R. Yanbarisov, and P. Zulian. Verification benchmarks for single-phase flow in three-dimensional fractured porous media. *Advances in Water Resources*, vol. 147, pp. 103759, 2021.

[3] K.-K. Phoon, S.-H. Chan, K.-C. Toh, and F.-H. Lee. Fast iterative solution of large undrained soil-structure interaction problems. *International Journal for Numerical and Analytical Methods in Geomechanics*, vol. 27, n. 3, pp. 159–181, 2003.

[4] O. Durán, P. R. Devloo, S. M. Gomes, and F. Valentin. A multiscale hybrid method for darcy's problems using mixed finite element local solvers. *Computer Methods in Applied Mechanics and Engineering*, vol. 354, pp. 213–244, 2019.
[5] D. Bertaccini and F. Durastante. *Iterative Methods and Preconditioning for Large and Sparse Linear Systems with Applications*. Chapman & Hall/CRC Monographs and Research Notes in Mathematics. CRC Press, 2018.
[6] L. Demkowicz, P. Monk, L. Vardapetyan, and W. Rachowicz. De rham diagram for hp finite element spaces. *Computers & Mathematics with Applications*, vol. 39, n. 7, pp. 29–38, 2000.
[7] P. R. B. Devloo. Pz: An object oriented environment for scientific programming. vol. 150, 1997.
[8] O. C. Zienkiewicz. Displacement and equilibrium models in the finite element method by b. fraeijs de veubeke, chapter 9, pages 145–197 of stress analysis, edited by o. c. zienkiewicz and g. s. holister, published by john wiley & sons, 1965. *International Journal for Numerical Methods in Engineering*, vol. 52, n. 3, pp. 287–342, 2001.
[9] B. Cockburn and J. Gopalakrishnan. A characterization of hybridized mixed methods for second order elliptic problems. *SIAM Journal on Numerical Analysis*, vol. 42, n. 1, pp. 283–301, 2004.
[10] B. Irons. Structural eigenvalue problems - elimination of unwanted variables. *AIAA Journal*, vol. 3, n. 5, pp. 961–962, 1965.
[11] R. J. Guyan. Reduction of stiffness and mass matrices. *AIAA Journal*, vol. 3, n. 2, pp. 380–380, 1965.